ELSEVIER

Polymer 42 (2001) 1121–1129

polymer

www.elsevier.nl/locate/polymer

XPS and AFM surface studies of solvent-cast PS/PMMA blends

C. Ton-That, A.G. Shard, D.O.H. Teare, R.H. Bradley*

Materials Surfaces and Interfaces Research Centre, School of Applied Sciences, The Robert Gordon University, St. Andrew Street, Aberdeen AB25 1HG, UK

Received 7 September 1999; received in revised form 23 February 2000; accepted 14 June 2000

Abstract

Films of polystyrene (PS) and poly(methyl methacrylate) (PMMA) blends of two different thicknesses have been examined by X-ray photoelectron spectroscopy (XPS) and atomic force microscopy (AFM). Blends with different compositions were spin-cast onto a mica substrate with chloroform as the mutual solvent. XPS measurements revealed surface enrichment of PMMA in all compositions. The thicker (66 nm) films exhibit a higher degree of PMMA surface enrichment than the thinner (17 nm) films. AFM imaging allows distinctions to be drawn between blends with differing compositions. The blend films with less than 50% PMMA bulk concentration generally exhibit pitted surfaces; the pit size varies with film thickness and bulk composition. When the PMMA bulk concentration is greater than 50%, the film surface changes to show island-like phase-separated structure. The surface segregation and morphology are explained in terms of solubilities of the two polymers in the solvent and dewetting of PMMA relative to PS. The phase domains on the film surface have also been resolved by frictional force microscopy (FFM) using hydrophilic tips bearing hydroxyl groups.

Keywords: Polymer blends; XPS; AFM

1. Introduction

Several miscible and immiscible polymer blend systems have previously been studied by other workers. Examples include polycarbonate/poly(methyl methacrylate) (PC/PMMA) [1,2]; poly(sebasic anhydride)/poly(DL-lactic acid) (PSA/PLA) [3]; poly(vinyl chloride)/poly(methyl methacrylate) (PVC/PMMA) [4]; and polystyrene/poly-(methyl methacrylate) (PS/PMMA) [5] blends. Immiscible blends are known to have properties which combine those of both the polymers, and also to have segregated structures with domains predominantly formed from the individual homopolymers. It has been shown that changing the relative homopolymer proportions in such blends varies the domain structure and surface morphology [3–5]. Another important aspect of immiscible blends is the tendency for one of the homopolymers to be enriched at the surface in preference to the other. In PC/PMMA blends, the surface segregation of PMMA has always been observed even when PC nodules are present in the bulk [2]. For PSA/PLA blends, the surfaces were enriched with PLA component at all compositions [3]. The driving forces for this surface enrichment can be caused by differences in the surface free energies of the polymer components [4,6]. In general, the component with lower surface free energy is enriched at the surface in order to minimise the polymer–air surface tension.

For immiscible polymer blends cast into films, the surface segregation and morphology may also be modified by different factors such as film thickness [5,7] and casting solvent [1]. If the blend films have a low thickness then polymer segregation can be promoted, as shown by Tanaka et al. [7] for the polystyrene/ poly(vinyl methyl ether) (PS/PVME) blends, leading to the formation of bilayer systems. Solvent-cast films may not be equilibrated thermodynamically due to the rapid solvent evaporation during the spin-casting process and the resulting surface could be predominantly due to solvent effects [8]. For PVC/PMMA blends, the surface was enriched with PMMA if blends were cast from tetrahydrofuran (THF), while surface composition was equivalent to the bulk if blends were cast from methyl-ethylketone [9]. PS/PMMA blend is a well-known immiscible combination for which bulk and surface phase separation has been observed [5,10]. In this study, we have cast the PS/PMMA films from chloroform solutions and analysed their surface chemistry and morphology by X-ray photoelectron spectroscopy (XPS) and atomic force microscopy (AFM), respectively. In addition, we have employed chemically modified AFM tips to probe the phase structure of the film surfaces via the apolar or polar natures of these polymers.

* Corresponding author. Tel.: +44-1224-262-822; fax: +44-1224-262-828.

E-mail address: r.bradley@rgu.ac.uk (R.H. Bradley).

0032-3861/01/$ - see front matter
PII: S0032-3861(00)00448-1

2. Experimental section

2.1. Preparation of polymer films

PS ($M_w = 280$K) and PMMA ($M_w = 350$K), were used as obtained (Sigma Aldrich, UK). Glass transition temperatures of the PS and PMMA, measured by differential scanning calorimetry, were 106 and 111°C, respectively. Polymer solutions were prepared by dissolving each polymer in chloroform, the concentration of the solutions is expressed as % weight/volume (% w/v). Polymer blend solutions were achieved by mixing solutions of the homopolymers in the desired proportions. Polymer films were prepared by spin-casting 60 μl aliquots of the polymer solutions under ambient conditions onto a freshly cleaved mica substrate, which was rotated at ~3000 r.p.m for 2 min. Mica was chosen as the substrate due to the ease with which large atomically flat areas can be obtained by cleaving.

In order to investigate the effects of film thickness on the surface morphology and surface chemistry of the blend films, films of differing thickness were cast by varying the concentration of the polymer solutions. Spin rate and all other parameters as described above were kept constant. Film thickness was evaluated by scratching through the polymer films by continual scanning of the AFM silicon tip at high loading force (~260 nN) with "slow-axis disabled" as described in our previous work on PS and PMMA films [11]. That study also includes a comparison with XPS angle-resolved thickness measurements for films of thickness <6 nm. In the work reported here the tip-scratch method has been used with the average depth of the scratches relative to the mean surface plane, corresponding to the film thickness, being measured by passive AFM re-imaging. The average thicknesses of the films cast from 1% and 0.2% w/v solutions were measured at ca. 66 ± 11 and 17 ± 4 nm, respectively.

2.2. Surface characterisation

Surface chemical compositions of the homopolymer films and their blends were measured by XPS using a Kratos Axis 5-channel HSi spectrometer with monochromated AlKα (1486.6 eV) X-rays operated at 150 W with the axis of the energy analyser normal to the plane of the sample surface. The sample analysis chamber of the XPS instrument was maintained at a pressure of $\sim 10^{-9}$ Torr. Charge neutralisation was used for all the samples to offset charge accumulation on surfaces. Elemental compositions were calculated from the areas of carbon 1s and oxygen 1s peaks in the survey spectra collected at a pass energy of 80 eV, and an energy resolution of approximately 1 eV, using appropriate relative sensitivity factors (errors approximated at ±5% by the analysis of reference clean PTFE tape). Detailed surface chemical composition was obtained by analysis of C 1s envelopes collected at a pass energy of 20 eV which gives an energy resolution of 0.45 eV. Chemical shift peaks are charge referenced to the C–C/C–H peak at 285 eV. Peak analysis was carried out using Kratos software and also version 1.5 of the Spectral Data processor (XPS International).

Surface topography of the films was characterised by AFM under ambient conditions, using a Digital Instruments (DI) Multimode SPM system. All imaging was performed in tapping-mode™ using silicon tips with cantilever driving amplitudes of 45–80 nm and feedback achieved at ~60% of the driving amplitude. Image analysis was performed using commercial DI software (version 4.23r3).

2.3. Frictional force microscopy (FFM)

In order to investigate tip-sample interactions on the frictional response of the polymer films, AFM tips bearing hydrophilic hydroxyl groups were employed. Procedures for cleaning and hydrophilisation of the AFM tips were carried out in accordance with the prescription of Ito et al. [12]. The Si_3N_4 cantilevers with integrated tip were exposed to ultraviolet-ozone (UVO) for 15 min in a Jelight 42-220 UVO cleaner. UVO treatment has been shown to effectively remove contaminants such as hydrocarbons [13], and will further oxidise the native oxide layer on the Si_3N_4 tip surface. After UVO treatment, the tips were first immersed in 0.5 M NaOH for 20 min, then in 0.1 M HCl for 10 min and finally in 0.5 M NaOH for 10 min. Subsequently, the tips were rinsed in Milli-Q deionised water (resistivity = 18.3 MΩ cm) and dried in a vacuum for 10 min at 100°C. This procedure has been reported to make the tip surface become more hydrophilic by increasing the surface concentration of silanol groups [12,14].

Frictional force imaging was performed simultaneously with topographical imaging in contact mode by scanning the tip in the direction orthogonal to the long cantilever axis. The probes used were standard 200 μm long V-shaped Si_3N_4 cantilevers with narrow legs (nominal spring constant 0.06 Nm^{-1}, nominal tip radius 20–60 nm [15]). Individual spring constants were determined using the method described previously by Cleveland et al. [16]. A constant scan rate of 6 μms^{-1} was used in all the FFM experiments. To allow meaningful comparisons of friction on the different films, the same tip was used for all the films tested. The laser alignment of each tip used was not altered throughout the experiments, as this has been found also to introduce relative errors [17]. To evaluate frictional forces, we analysed line profiles of the forward and reverse scans, i.e. friction loops [18,19]. The friction at a given load was evaluated as half the difference between forward and reverse lateral signals. Except where specified, the loads in this paper refer to externally applied loads, i.e. the product of calibrated spring constant with cantilever displacement. Cantilever displacements were measured relative to the point where 'jump to contact' occurs. The possible influence of capillarity was removed by undertaking all lateral force imaging under fluid [20]. Decane ($C_{10}H_{22}$) was chosen as

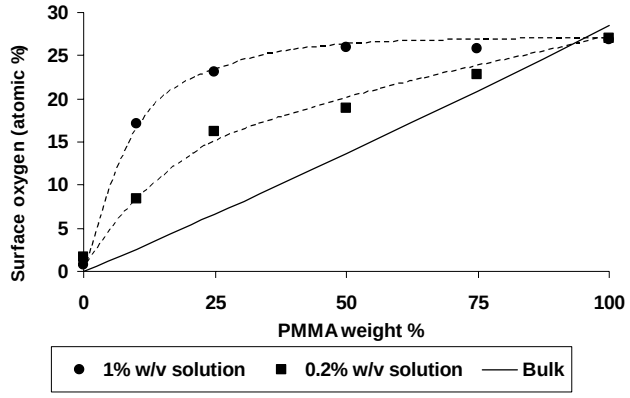

Fig. 1. Comparison of surface oxygen concentration with bulk weight percent of PMMA for films cast from 1 and 0.2% w/v solution. The solid line shows the calculated oxygen concentrations of the bulk.

the medium for all FFM experiments due to its non-polarity, which also eliminates any electrostatic double-layer interaction forces between the polymer surface and probe-tip [21]. In addition, it is a non-solvent for both of the polymers and convenient to use in AFM experiments because of its high boiling point (174°C) and low toxicity.

3. Results and discussion

3.1. Surface compositions (XPS)

XPS survey spectra of all the polymer films demonstrate the presence of only two elements, carbon and oxygen, no signals indicative of the mica substrate being present. A comparison of the experimentally determined surface oxygen concentration with the bulk weight percent of the PMMA, for the films cast from 1 and 0.2% w/v solutions, is shown in Fig. 1. The solid line is the calculated bulk oxygen concentration, which increases almost linearly with the weight percent of the PMMA. The surface oxygen concentration measured on the PMMA film was 26.3 atomic%, which is close to the stoichiometric value of 28.6 atomic%. The non-linearity of the graph, which is due to relatively high levels of oxygen at low PMMA percent, indicates that there is an excess of the PMMA at the surface in both types of the blend film. The thicker films (66 nm thick), however, show a higher surface oxygen concentration than the thinner films (17 nm thick), indicating a higher degree of PMMA surface enrichment for the former.

The high-resolution carbon 1s (C 1s) and oxygen 1s (O 1s) spectra of the pure PS and PMMA films were in excellent agreement with previously published work [22]. Typical C 1s spectra obtained with the two pure polymer films and for the blend film cast from a 0.2% w/v solution containing 50% PS: 50% PMMA are shown in Fig. 2. The deconvolution results of the C 1s envelopes obtained without applying any constraints for the two polymers are presented in Table 1. The C 1s spectrum of the PS film includes a main hydrocarbon peak at binding energy of 285.0 eV and $\pi-\pi^*$ shake-up satellites at shifts of 6–8 eV from the hydrocarbon peak. The C 1s envelope of the PMMA film can be resolved into four components: hydrocarbon (C–C/C–H) at a binding energy of 285.0 eV, β-shifted carbon (due to their juxtaposition to O–C=O groups) at 285.7 eV, methoxy group-carbon at 286.8 eV and carbon in the ester group at 289.1 eV. As shown in Table 1, the percentages of the different contributions are close to the expected stoichiometric values of the two polymers (in all cases, the agreement is within 2%). The full-width at half maximum (FWHM) values of those four contributions in PMMA are in the range between 0.94 and 1.12 eV. Similar variations in these FWHM values have also been observed by other authors [2,22].

For quantitative analysis of the surface composition for the blend films two methods were used by considering either the elemental O/C ratio from survey spectra or the relative ester contribution to the C 1s envelopes. The ester peak at 289.1 eV was specifically chosen for this purpose because it does not significantly overlap any other peak and contains contribution solely from PMMA. The experimental O/C ratio contains the contribution of each polymer to the overall O 1s and C 1s spectra, which can be expressed as

$$\left(\frac{O}{C}\right)_{\text{exp}} = \frac{XO_{\text{PMMA}}}{XC_{\text{PMMA}} + (1-X)C_{\text{PS}}} \tag{1}$$

where X is the molar PMMA surface concentration in the blend and O_{PMMA}, C_{PMMA} and C_{PS} are the stoichiometric oxygen and carbon atomic concentrations in pure PMMA and pure PS, respectively. Rearranging Eq. (1), we have:

$$X = \frac{8(O/C)_{\text{exp}}}{3(O/C)_{\text{exp}} + 2} \tag{2}$$

In order to check the consistency of the XPS results, the PMMA molar concentration X at the surface was also evaluated from the percentage of the ester group in the C 1s envelopes. Since in the blend the relative contribution of PMMA in the C 1s intensity is $5X$ (five carbon atoms per PMMA repeat unit) and that of PS is $8(1\text{-}X)$ (eight carbon atoms per PS repeat unit), we have

$$\left(\frac{I_{\text{O=C–O}}}{I_{\text{C}}}\right)_{\text{exp}} = \frac{X}{5X + 8(1-X)} \tag{3}$$

Rearranging Eq. (3) gives:

$$X = \frac{8(I_{\text{O=C–O}}/I_{\text{C}})_{\text{exp}}}{3(I_{\text{O=C–O}}/I_{\text{C}})_{\text{exp}} + 1} \tag{4}$$

The surface PMMA concentrations evaluated using the above methods are presented in Fig. 3 as a function of the PMMA bulk molar concentration. It can be seen that the agreement between the two methods is relatively good (in most cases, the discrepancy was within 5%). This discrepancy may be explained by different factors:

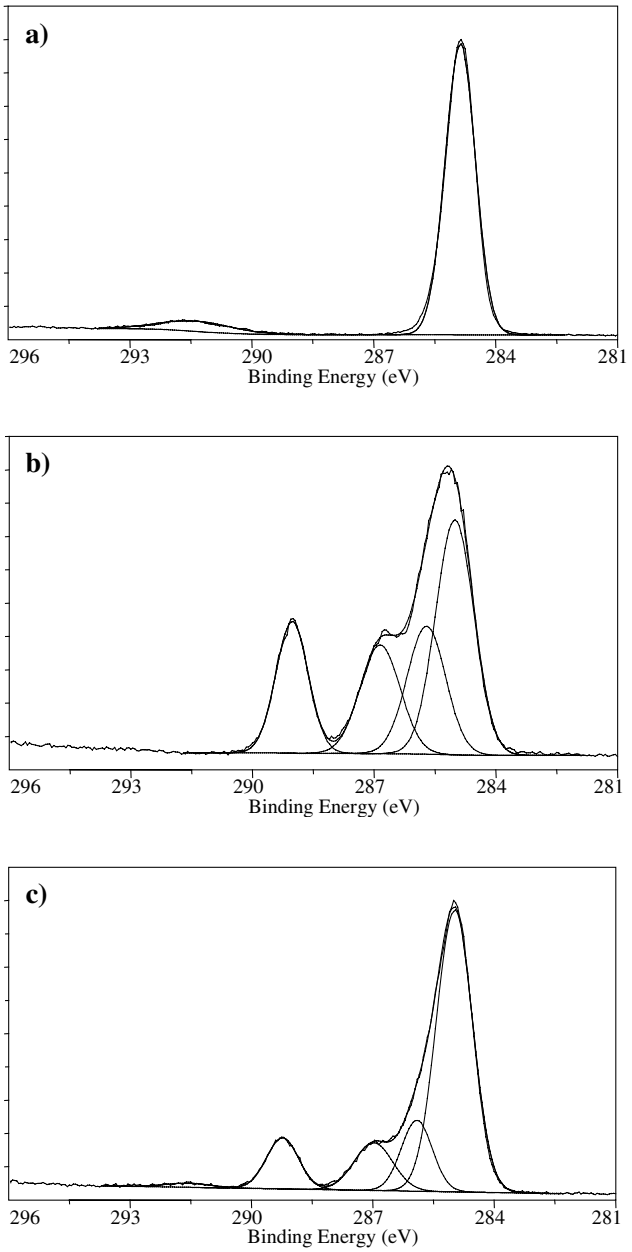

Fig. 2. High-resolution C 1s spectra with fitted curves for: (a) PS; (b) PMMA; and (c) 50% PS: 50% PMMA blend films cast from 0.2% w/v solutions.

Table 1
XPS parameters for two pure polymers

	Peak	Binding energy (eV)	FWHM (eV)	Atomic%
PS	C–C/C–H	285.0	0.89	92.3
	$\pi \rightarrow \pi^*$	291.5	2.12	7.7
PMMA	C–C/C–H	285.0	1.11	39.9
	β-shifted C	285.7	1.12	21.9
	C–O	286.8	1.16	19.3
	O–C=O	289.1	0.94	18.9

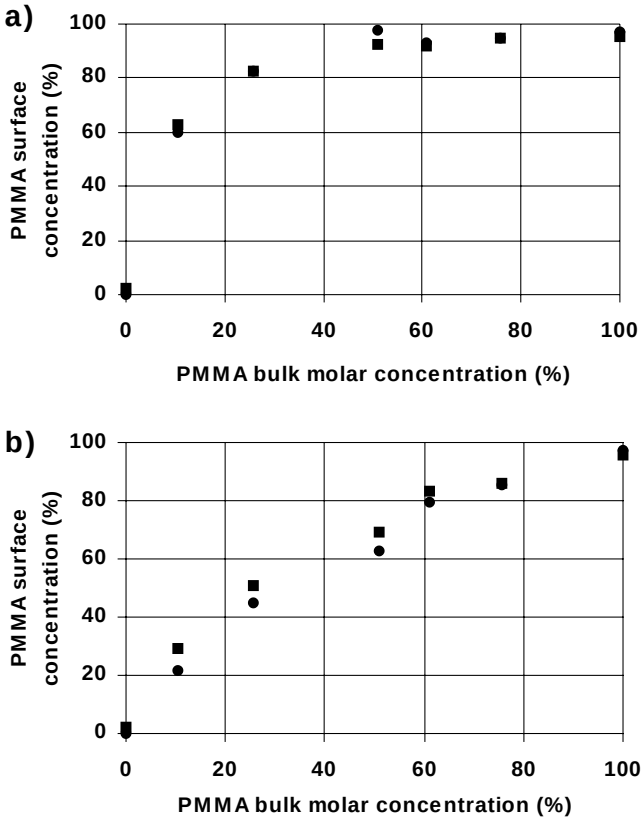

Fig. 3. Surface concentration of PMMA in the blends calculated by means of elemental O/C ratio (■) and relative ester peak intensity (●) as a function of the PMMA bulk concentration. Films were cast from: (a) 1% w/v solutions; (b) 0.2% w/v solutions. The greater PMMA surface enrichment of the 1% w/v film is clear.

(a) difference in XPS sampling depths of C 1s and O 1s photoelectrons, resulting in an inaccurate experimentally determined O/C ratios at heterogeneous surfaces; (b) surface hydrocarbon contamination; and (c) errors in curve fittings of the XPS spectra. Again, there is clear indication that there is a surface excess of PMMA in both types of the films.

The degree of PMMA enrichment at the surface is higher in the thicker films cast from 1% w/v solutions. For a bulk molar concentration of 26% PMMA, the surface PMMA concentrations for the films cast from 1 and 0.2% w/v solutions are 83 and 44%, respectively (quantification using the ester group). For the 1% w/v blend films, the PMMA surface molar concentration first increases steeply with the PMMA bulk molar concentration (the surface concentration reaches 60% of PMMA for a 10% bulk concentration), then increases slowly and saturates at ca. 96% for a 51% bulk concentration (Fig. 3(a)). These results show clearly that the PS component is excluded almost completely from the surface for films, which were cast from 1% w/v solution with a molar concentration of PMMA greater than 51%. In the 0.2% w/v blend films, the PMMA surface concentration increases more linearly as the bulk concentration varies from 0 to 100% PMMA concentration (Fig. 3(b)). This

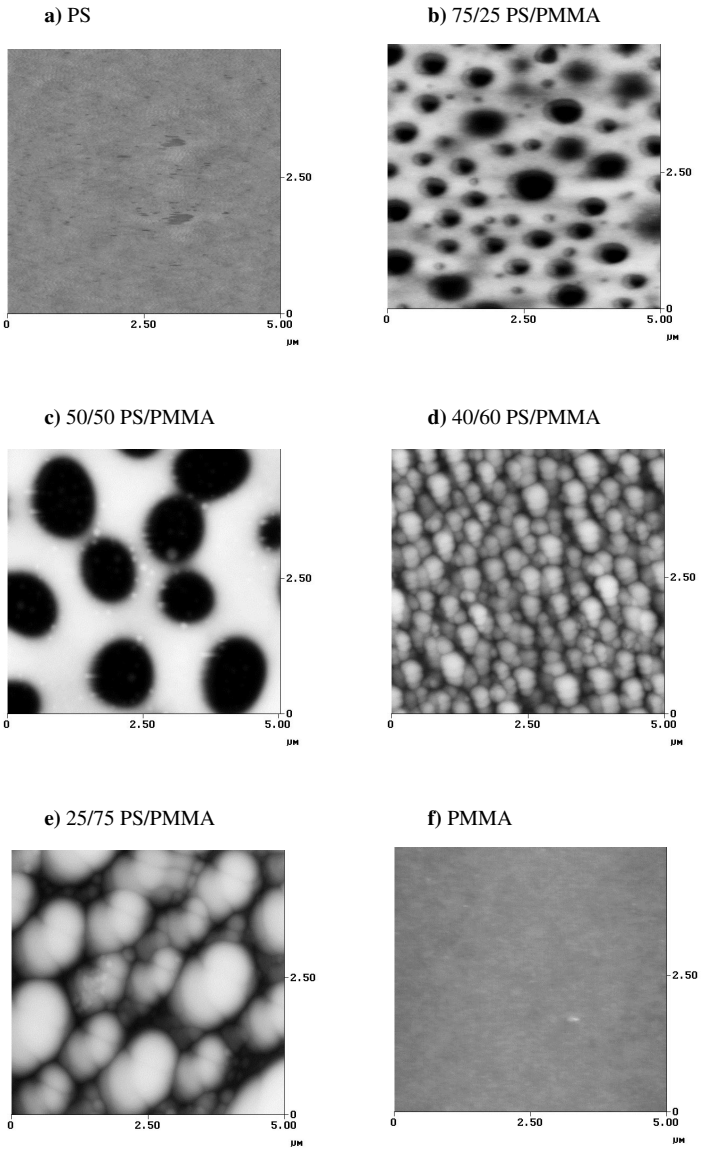

Fig. 4. AFM images of the surface topography of PS and PMMA in single component and blended thin films cast from 1% (w/v) solution.

indicates a stronger PMMA surface segregation occurring in the thicker (66 nm) film.

3.2. Surface morphology (AFM)

The thin films of pure PS and PMMA and the blends containing different proportions of the polymers all display differing and distinct surface morphologies when analysed with AFM. Fig. 4 shows typical $5 \times 5\ \mu m^2$ areas of the films that were cast from 1% w/v solutions. The pure polymer films, shown in Fig. 4(a) and (f), exhibit flat surfaces with few surface features: RMS roughness measured on a $5 \times 5\ \mu m^2$ area was 0.7 ± 0.2 nm for both PS and PMMA films. For the polymer blends containing 75% PS: 25% PMMA, the AFM topography shows a pitted surface (Fig. 4(b)). The pits have a broad, shallow structure with typical diameter ranging from 300 to 600 nm and depths of between 15 and 25 nm. A pitted surface morphology, as shown in Fig. 4(c), was also observed for the 50% PS: 50% PMMA film. The pits are larger than those in the 75% PS: 25% PMMA film, their diameter being between 1.2 and 1.6 μm with depths of 30–40 nm. When the polymer composition is changed to 40% PS: 60% PMMA, the surface tends to show a granular morphology (Fig. 4(d)). The granules have diameters of about 400 nm and protrude above the surface material by 15–30 nm. With 25% PS: 75% PMMA film, the topography also shows a granular surface, but the granules are larger in size with diameters of about 1–1.3 μm. Between the granules, the polymer film appears to be continuous.

AFM images of the polymer films cast from 0.2% w/v solutions are shown in Fig. 5. The pure PS and PMMA films again display smooth surface topography (Fig. 5(a) and (f)). The surfaces of the 0.2% w/v blend films show some

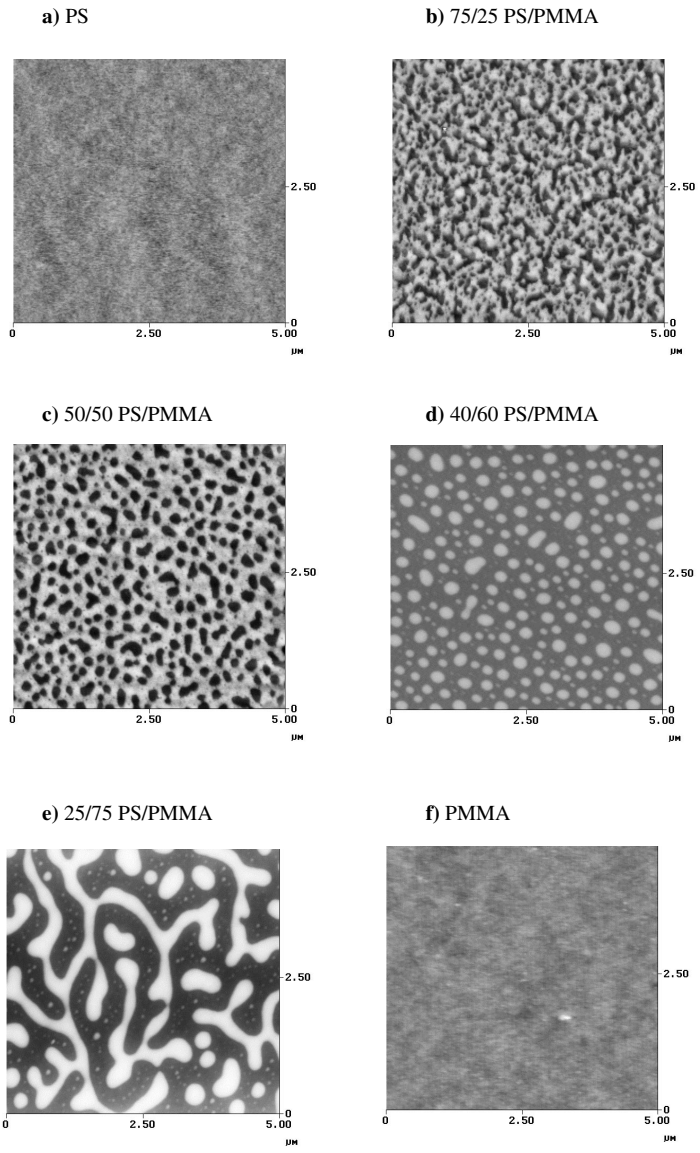

Fig. 5. AFM images of the surface topography of PS and PMMA in single component and blended thin films cast from 0.2% (w/v) solution.

similarity to the 1% w/v films with the same mixing PS/PMMA ratio. With the 75% PS: 25% PMMA and 50% PS: 50% PMMA films, the surfaces show pitted topography as seen in Fig. 5(b) and (c), but the pits are much smaller and shallower compared to those of the 1% w/v films. Many of these pits are interconnected. Fig. 5(d) shows the topography of the 40% PS: 60% PMMA film, which exhibits a well-defined island structure. These isolated islands have a height of about 5–11 nm above the continuous surface and a diameter of about 150 nm. When the film composition is changed to 25% PS: 75% PMMA, the islands tend to coalesce together to form large and continuous islands, as seen in Fig. 5(e). Since the island area fraction increases with PMMA bulk concentration, these islands are most probably composed of a PMMA-rich phase.

3.3. Frictional force microscopy results

Frictional forces between the hydroxylated tip and the two polymers have been evaluated over the loading range 0–75 nN. Surface wear was not observed on the polymer films when imaging within this loading regime. Fig. 6 shows the variation of averaged frictional forces as a function of normal load, as measured on the pure PS and PMMA surfaces. As is clear from these data, the frictional forces are higher for the PMMA film than the PS film at the same applied load. The frictional force increases almost linearly with load for both of the polymer films. The general frictional behaviour of the PS and PMMA films studied here is similar to that reported for various AFM tips and polymer surfaces [23,24]. Although we do not know the exact values of the frictional forces (since torsional spring constants are

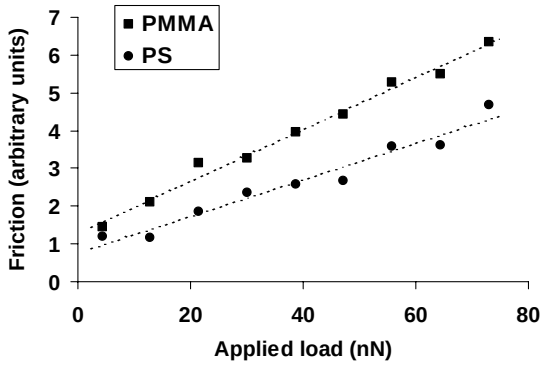

Fig. 6. Friction force versus applied load data recorded for pure PS and PMMA films using a hydroxylated tip.

not accurately known), the *relative* friction coefficients could be accurately (±10%) determined. The friction coefficient of the PMMA film is ca. 1.5 times that of the PS film. Since the elastic moduli of the two polymers are similar (3200 and 3300 MPa for PS and PMMA [25], respectively) the higher friction measured on the PMMA is likely due to polar interactions between the hydroxylated tip and polymer surface as reported in the previous work [23].

Fig. 7(a) shows topographical and frictional force images

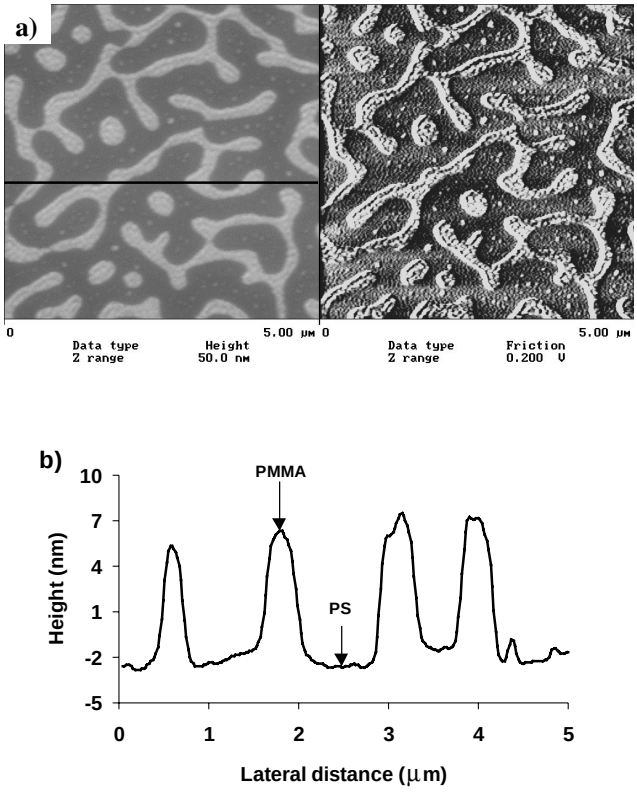

Fig. 7. (a) Topographic (left) and frictional (right) images of 25% PS: 75% PMMA film cast from 0.2% w/v solution. The images were collected simultaneously using a hydroxylated tip. Frictional image reveals higher friction (light contrast) in the islands, which are PMMA-rich domains. (b) Sectional view of the film.

of the 25% PS: 75% PMMA film cast from a 0.2% w/v solution. The friction image was collected simultaneously with topography using a hydroxylated tip in decane medium at an applied load of ca. 52 nN. The frictional image reveals higher friction (light contrast) within continuous islands and lower friction (dark contrast) in the surface matrix. Frictional contrast between the two polymers has been reported previously [26]; friction with unmodified Si_3N_4 tip was found to be lower for PS at an applied load of 10 nN but the contrast was eliminated upon decreasing the applied load. The surface morphology was also examined by phase-detection imaging in tapping mode AFM, but no contrast was detected. This is probably due to similar elastic properties of the two polymers [27]. The height profile along the line in the topographic image is also shown in Fig. 7(b). The islands are PMMA-rich domains, which exhibit higher friction than the PS-rich phase when imaging using the polar (hydroxylated) tip. In the PS-rich phase small droplet-like domains of PMMA are visible, indicating that complete phase separation has not occurred. In the case of the 25% PS: 75% PMMA film cast from a 1% w/v solution, FFM revealed no difference in the contrast between the granules and rest of the image (not shown), indicating a single phase at the surface. This is consistent with the XPS results, which show that the surface is almost completely covered with PMMA. Moreover, for the blend films with PMMA concentrations of 50% or less FFM also reveals same contrast in the pits and the surrounding matrix, suggesting that the whole surface is composed of a single phase.

4. Discussion

The solvent-cast films in these studies are probably not at thermodynamic equilibrium due to the rapid solvent evaporation in the spin-casting process. Although PS has a marginally lower surface free energy than PMMA ($\gamma = 40.2$ and 41.2 mJ m^{-2} for PS and PMMA [5], respectively), it is excluded from the air–polymer interface. It is possible to explain this PMMA surface enrichment in terms of solvent effects [5]. Due to a higher solubility of the PMMA in the chloroform, PS is more quickly depleted from the solvent and solidifies first onto the substrate. PMMA tends to stay longer in the liquid phase and forms a second layer at the surface. This bilayer-segregated system has also been observed for the PS/PMVE blend films [7]. In our work, surface enrichment of PMMA has been observed by XPS in all the blend films. The PMMA concentration at the surface is always higher than that in the bulk, regardless of the film thickness. It appears that the thicker film (as controlled by the polymer concentration of the cast solutions) possess a higher degree of PMMA surface enrichment. This may be due to the formation of a thicker and/or more continuous surface overlayer of PMMA.

The morphology of blend surfaces appears to fall into three distinct categories. With PMMA concentrations of

50% or less a pitted surface is observed, the size of the pits increases both with film thickness and PMMA concentration. At higher concentrations of PMMA the 17 nm thick films display a surface morphology similar to that observed previously for films of a comparable composition [5], whereas the thicker films showed a granular surface with the granule size increasing with PMMA concentration.

The films formed with a composition of less than 50% PMMA concentration display similarly pitted features albeit on different scales. This would suggest that there are common factors involved in the development of these morphologies. XPS data reveals that the surfaces are enriched with PMMA to an extent inconsistent with the ratio of matrix to pit areas determined from AFM. Additionally FFM indicates that the composition of the pits is not substantially different from the surrounding matrix material. These observations indicate that the pit surfaces do not consist of a PS rich phase, but that the whole surface comprises of a single PMMA rich phase. In the films where PS is observed by XPS it is probably subsurface but within the sampling depth of the XPS technique. The pits are probably associated with subsurface formations of PS, and this leads us to consider two possible models for these systems, which are shown in Fig. 8(a) and (b). In model 8(a) the pits in the PMMA overlayer are coincident with hills in the PS underlayer. In this model the thickness of the PMMA overlayer varies between the pits and the surrounding matrix areas and the PMMA surface is a negative relief map of the PS/PMMA interface. Model 8(b) describes a system in which the PMMA surface directly conveys the PMMA/PS interface topography. The PMMA overlayer shown in Fig. 8(b) varies in thickness, but this is not a necessary feature of the model.

Both of the models 8(a) and (b) bear similarities to collective oscillations in stratified liquids [28], Fig. 8(a) corresponding to a longitudinal peristaltic mode and Fig. 8(b) a transverse bending mode. These oscillations are of importance when the dynamics of dewetting are considered, and it is found that for unstable liquid films certain peristaltic modes are amplified leading to film rupture and dewetting [28]. The formation of the pitted structures may occur via the initial production of a bilayer solution of PMMA on top of a solution of PS. The PMMA layer is unstable and begins to dewet from the PS layer, however chloroform evaporation increases the viscosity of both layers and dewetting is not completed within the timescale of the solvent evaporation.

If this view is valid, one should expect the size of the surface features to be proportional to the square of the average PMMA overlayer thickness. This is due to the rapid amplification of selected peristaltic modes [28]. An estimate of PMMA film thickness can be obtained from the product of the mole fraction of PMMA and the blend thickness. Using this approximation the surface feature dimensions would be expected to increase in the order (75/25 17 nm) < (50/50 17 nm) < (75/25 66 nm) < (50/50 66 nm) which is the observed order. Furthermore, the feature size (average pit diameter) is predicted to increase by a factor of approximately four for each step in the series given above and this is in good agreement with the experimental results.

Quite different surface morphologies are observed when the PMMA mole fraction is above 50%. In this regime the partial dewetting model described above for the low PMMA mole fraction surfaces no longer appears valid. For the thin films XPS indicates the presence of PS in the film surface and FFM also strongly suggests that for the 25% PS: 75% PMMA blend the PS domains extend to the top surface of the solid blend. This would indicate that the dewetting/phase separation of PS and PMMA rich phases has reached a stage of greater completion than films with lower PMMA concentrations. Complete dewetting may result from the blend mix having greater solubility in or retention of chloroform solvent with higher PMMA fractions. Greater completion of the dewetting of model 8(a) will result in model 8(c), which is virtually identical to the model proposed by Tanaka et al [5] for surfaces similar to those discussed here. In their work, more complete dewetting was probably due to toluene being used as cast solvent, which is less volatile than chloroform used in this study.

The granular surfaces seen for thicker films of greater than 50% PMMA mole fraction appear to bear little structural relationship to the other blend films. It is possible that the features arise from very closely packed domains of

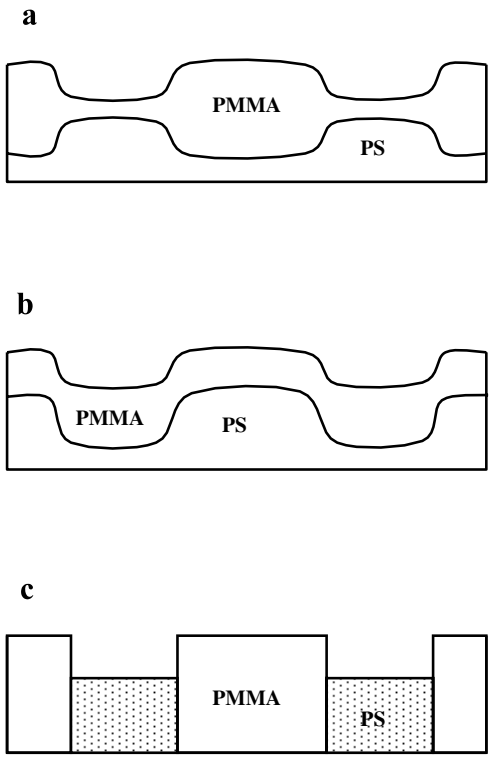

Fig. 8. Structural models of PS/PMMA blends: (a) surface pits correspond to hillocks in PS–PMMA interface; (b) surface pits correspond to pits in PS–PMMA interface; and (c) complete dewetting of the PS underlayer from model (a). See text for discussion.

PMMA or from the deposition of colloidal particles produced in solution during the spin casting process.

5. Conclusions

Surface analysis of the PS/PMMA blends has recorded both surface enrichment and phase separation. XPS reveals that in all the blends investigated the surface is always enriched with the PMMA component. This surface segregation occurs more strongly in the thicker (66 nm) film than in the thinner (17 nm) film. AFM has contrasted the surface morphology of blends with differing compositions; both pitted and granular topographies have been observed depending on the bulk composition. Surface phase-separated structure has been recorded by frictional force microscopy using polar (hydroxylated) tips for the thin films with PMMA concentrations of more than 50%. The formation of blend morphology can be explained by two factors: difference in the solubility of the two polymers in the solvent and dewetting of PMMA-rich domains from the PS-rich phase.

Acknowledgements

C.T.T. acknowledges the Robert Gordon University for a research studentship.

References

[1] Chiou JS, Barlow JW, Paul DR. J Polym Sci Part B, Polym Phys 1987;25:1459–71.
[2] Lhoest JB, Bertrand P, Weng LT, Dewez JL. Macromolecules 1995;28:4631–7.
[3] Davies MC, Shakesheff KM, Shard AG, Domb A, Roberts CJ, Tendler SJB, Williams PM. Macromolecules 1996;29:2205–12.
[4] Jackson ST, Short RD. J Mater Chem 1992;2:259–60.
[5] Tanaka K, Takahara A, Kajiyama T. Macromolecules 1996;29:3232–9.
[6] Jones RAL, Kramer EJ, Rafailovich MH, Sokolov J, Schwarz SA. Phys Rev Lett 1989;62:280–3.
[7] Tanaka K, Takahara A, Kajiyama T. Macromolecules 1995;28:934–8.
[8] Garbassi F, Morra M, Occhiello E. Polymer surfaces: from physics to technology. Chichester, UK: Wiley, 1998 (p. 291).
[9] Schmidt JJ, L GJA. Salvati. Macromolecules 1989;22:4489.
[10] Kessler J, Higashida N, Shimomai K, Inoue T, Ougizawa T. Macromolecules 1994;27:2448.
[11] Ton-That C, Shard AG, Bradley RH. Langmuir 2000;16:2281–4.
[12] Ito T, Namba M, Buhlmann P, Umezawa Y. Langmuir 1997;13:4323–32.
[13] Vig JR. J Vac Sci Technol, A-Vacuum Surfaces and Films 1985;3:1027–34.
[14] Ogbuji LUT, Jayne DT. J Electrochem Soc 1993;140:759–66.
[15] Digital Instruments, Santa Barbara, CA, USA.
[16] Cleveland JP, Manne S, Bocek D, Hansma PK. Rev Sci Instrum 1993;64:403–5.
[17] Hu J, Xiao XD, Ogletree DF, Salmeron M. Surface Sci 1995;327:358–70.
[18] Overney RM, Takano H, Fujihira M, Paulus W, Ringsdorf H. Phys Rev Lett 1994;72:3546–9.
[19] Overney R, Meyer E. MRS Bull 1993;18:26–34.
[20] Grigg DA, Russel PE, Griffith JE. J Vac Sci Technol A 1992;10:680.
[21] Feldman K, Tervoort T, Smith P, Spencer ND. Langmuir 1998;14:372–8.
[22] Beamson G, Briggs D. High resolution XPS of organic polymers. Chichester, UK: Wiley, 1992.
[23] Ton-That C, Campbell PA, Bradley RH. Langmuir 2000;16:5054–8.
[24] Beake BD, Ling JSG, Leggett GJ. J Mater Chem 1998;8:2845–54.
[25] Brandrup J, Immergut EH, Grulke EA. Polymer handbook. 4th ed. New York: Wiley, 1999.
[26] Krausch G, Hipp M, Boltau M, Marti O, Mlynek J. Macromolecules 1995;28:260–3.
[27] Magonov SN, Elings V, Whangbo MH. Surface Sci 1997;375:L385–91.
[28] Brochard-Wyart F, Martin P, Redon C. Langmuir 1993;9:3682–90.